MS19378, JULY 1, 2005
Preprint typeset using LaTeX style emulateapj v. 6/22/04

CONFINED AND EJECTIVE ERUPTIONS OF KINK-UNSTABLE FLUX ROPES

T. TÖRÖK [1] AND B. KLIEM [2]

Received 2005 March 4; accepted 2005 July 18

ABSTRACT

The ideal helical kink instability of a force-free coronal magnetic flux rope, anchored in the photosphere, is studied as a model for solar eruptions. Using the flux rope model of Titov & Démoulin (1999) as the initial condition in MHD simulations, both the development of helical shape and the rise profile of a confined (or failed) filament eruption (on 2002 May 27) are reproduced in very good agreement with the observations. By modifying the model such that the magnetic field decreases more rapidly with height above the flux rope, a full (or ejective) eruption of the rope is obtained in very good agreement with the developing helical shape and the exponential-to-linear rise profile of a fast coronal mass ejection (CME) (on 2001 May 15). This confirms that the helical kink instability of a twisted magnetic flux rope can be the mechanism of the initiation and the initial driver of solar eruptions. The agreement of the simulations with properties that are characteristic of many eruptions suggests that they are often triggered by the kink instability. The decrease of the overlying field with height is a main factor in deciding whether the instability leads to a confined event or to a CME.

Subject headings: Instabilities – MHD – Sun: corona – Sun: flares – Sun: coronal mass ejections (CMEs)

1. INTRODUCTION

Large-scale solar eruptions occur as flares, filament (or prominence) eruptions, and coronal mass ejections (CMEs). Despite their different observational appearance, it is believed that these phenomena are manifestations of the same physical processes, which involve the disruption of the coronal magnetic field. Indeed, in the largest eruptions (eruptive flares) usually all three phenomena are observed. The theory of the main phase of such events, referred to as the "standard model" of eruptive flares (e.g., Shibata 1999), is quite well established. However, their initiation as well as the mechanism of upward acceleration are still unclear. A variety of theoretical models have been proposed to explain the impulsive onset and initial evolution of solar eruptions (see, e.g., Forbes 2000).

Here we focus on a flux rope instability model. This is motivated by the observation that solar eruptions often show the phenomenology of a loop-shaped magnetic flux system with fixed footpoints at the coronal base and signatures of magnetic twist. Furthermore, erupting filaments very often develop a clearly helical axis shape in the course of the eruption, which is the characteristic property of the helical kink instability of a twisted magnetic flux rope. The instability occurs if the twist, a measure of the winding of the field lines about the flux rope axis, exceeds a critical value (Hood & Priest 1981).

In coronal applications, the simplifying assumption of straight, cylindrically symmetric flux ropes has nearly always been used so far. Only very recently, Török, Kliem, & Titov (2004, hereafter Paper I) performed the first detailed study of the kink instability of an arched flux rope, line-tied to the photosphere, using the analytical model of a force-free coronal flux rope developed by Titov & Démoulin (1999, hereafter TD) as the initial condition in 3D ideal MHD simulations. They have shown that this model relaxes to a numerical equilibrium very close to the analytical expressions in the case of subcritical twist and that the helical kink instability develops for supercritical twist (see also Fan & Gibson 2003, 2004).

[1] Mullard Space Science Laboratory, University College London, Holmbury St. Mary, Dorking, Surrey RH5 6NT, UK; tt@mssl.ucl.ac.uk
[2] Astrophysical Institute Potsdam, An der Sternwarte 16, 14482 Potsdam, Germany; bkliem@aip.de

In the course of the instability, a helical current sheet, wrapped around the kinking and rising flux rope where it pushes into the surrounding field, and a vertical current sheet below the rope (which has no counterpart in the cylindrically symmetric case) are formed. A vertical current sheet below rising unstable magnetic flux is the central element in the standard model of eruptive solar flares. Further essential features of solar eruptions could be reproduced in the simulations, as for example the formation of transient soft X-ray sigmoids (Kliem, Titov, & Török 2004, Paper II). However, a full eruption of the configuration has not yet been obtained; the flux rope reached an elevation of only about twice its initial height.

Here we present further developments of these simulations to substantiate our suggestion in Papers I and II that the kink instability of a coronal magnetic flux rope is a possible trigger mechanism of solar eruptions. The instability was first suggested as the trigger of (confined and ejective) prominence eruptions by Sakurai (1976), but has recently been generally regarded as a possible explanation only for confined events (e.g., Gerrard & Hood 2003). The new simulations show that the instability can also trigger full eruptions.

2. NUMERICAL MODEL

We integrate the compressible ideal MHD equations using the simplifying assumptions of vanishing plasma-beta, $\beta = 0$, and vanishing gravity, which are identical to Eqs. (2–5) in Paper I. Setting $\beta = 0$ is usually a very good approximation in the lower and middle corona of active regions, the source region of most eruptions, where estimates yield $\beta \sim 10^{-3} \ldots 10^{-2}$. Both the pressure gradient force and the gravity force influence the rise characteristics of the unstable flux rope and the energy partition in the development of the instability. However, the basic characteristics of the instability are well described by the equations used whenever the Lorentz force dominates, as is the case in the initial phase of solar eruptions. Magnetic reconnection occurs in the simulations due to numerical diffusion if current sheets steepen sufficiently.

As in Papers I and II, we use the approximate analytical force-free equilibrium of an arched, line-tied, and twisted flux rope by TD as the initial condition for the magnetic field. The flux rope is modelled by the upper section of a toroidal

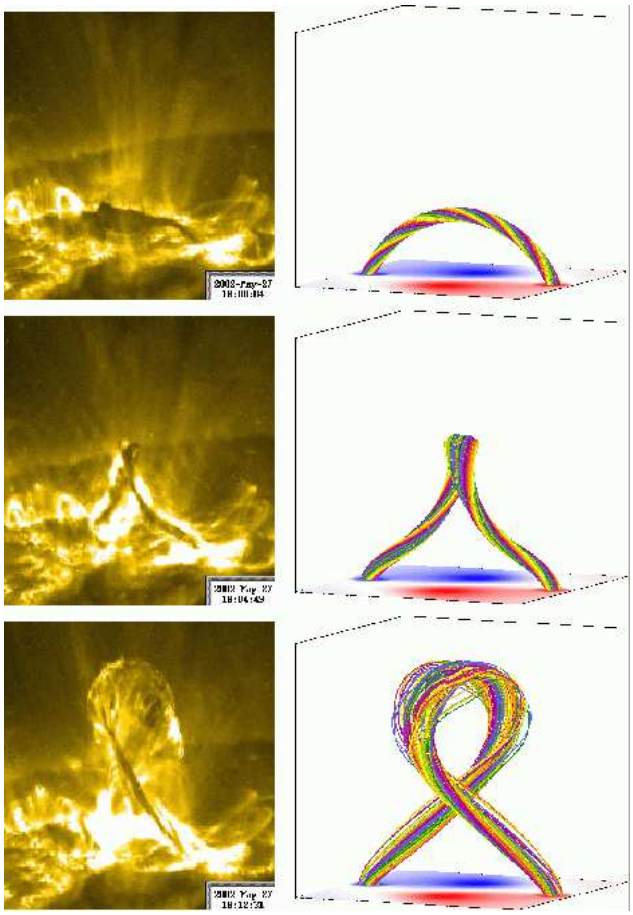

FIG. 1.— *Left: TRACE* 195 Å images of the confined filament eruption on 2002 May 27. *Right:* magnetic field lines outlining the core of the kink-unstable flux rope (with start points in the bottom plane at circles of radius $b/3$) at t = 0, 24, and 37. The central part of the box (a volume of size 4^3) is shown, and the magnetogram, $B_z(x,y,0,t)$, is included.

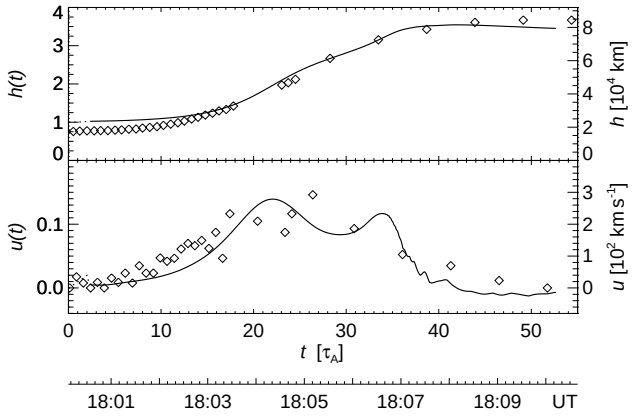

FIG. 2.— Comparison of height, $h(t)$, and velocity, $u(t)$, of the flux rope apex in the simulation (solid lines; initial perturbation is dotted) with the corresponding values of the filament eruption in Fig. 1 (data from Fig. 3 of Ji et al. [2003]) overplotted as diamonds (the height data observed before 18:04 UT were smoothed here, resulting in reduced velocity scatter). See text and Table 1 for the scaling of the dimensionless simulation variables (left axes) to the observed values (right axes).

ring current, partly submerged below the photosphere, whose Lorentz self-force is balanced by a pair of fictitious subphotospheric magnetic charges. A fictitious subphotospheric line current at the toroidal symmetry axis is included to achieve a finite twist everywhere in the system. See TD for a detailed description of the model.

The initial density distribution can be freely specified; we choose it such that the Alfvén velocity in the volume surrounding the flux rope decreases slowly with height: $\rho_0 \propto |\mathbf{B}_0(\mathbf{x})|^{3/2}$ (see Fig. 3 below). The system is at rest at t = 0, except for a small upward velocity perturbation, which is localized at the flux rope apex in a sphere of radius equal to the minor radius, b, of the rope. Lengths, velocities, and times are normalized, respectively, by the initial flux rope apex height, h_0, the initial Alfvén velocity at the apex, v_{A0}, and the corresponding Alfvén time, $\tau_A = h_0/v_{A0}$.

3. SIMULATION OF A CONFINED ERUPTION

The eruption of an active region filament (on 2002 May 27), which was accompanied by an M2 flare but did not lead to a CME, was described by Ji et al. (2003). The filament started to rise rapidly and developed a clear helical shape, as is often observed; however, the ascent was terminated at a projected height of $\approx$ 80 Mm (Figs. 1, 2). Such confined filament eruptions are not uncommon (Rust 2003).

In order to model this event, we consider a kink-unstable configuration which is very similar to the case of an average flux rope twist of 4.9π studied in detail in Paper I. The line current is reduced by about one third to enable a higher rise, but the average twist, $\Phi = 5.0\pi$ here, is kept to reproduce the helical shape. (In the TD model, this fixes the minor radius to b = 0.29, 8 percent larger than in the reference run in Paper I.) The sign of the line current is chosen to be positive to conform to the apparent positive (right-handed) helicity of the observed filament. Furthermore, we increase the numerical diffusion and prevent the density from becoming negative, which permits us to follow the evolution of the system for a considerably longer time. Otherwise, the magnetic configuration and the numerical settings are the same as in Paper I.

As in our previous simulations, the upwardly directed kink instability leads to the ascent and helical deformation of the flux rope as well as to the formation of current sheets (see Fig. 3 in Paper I). In Fig. 1 we compare the evolution of the helical shape of the flux rope with *Transition Region and Coronal Explorer (TRACE)* observations of the filament eruption. The evolution is remarkably similar. Figure 2 shows that the principal features of the observed rise are also matched. After an exponential rise the flux rope comes to a stop at $\approx 3.5\ h_0$. A first deceleration occurs as the current density in the helical current sheet above the apex begins to exceed the current density in the flux rope ($t > 22$). The subsequent upward push ($t > 30$) results from the reconnection outflow in the vertical current sheet below the rope. Finally, the rise is terminated by the onset of magnetic reconnection in the current sheet above the rope, which progressively cuts the rope field lines ($t \gtrsim 33$). The reconnection outflows expand the top part of the rope in lateral direction, as seen both in observation and simulation.

Using the scaling to dimensional values given in Table 1, good quantitative agreement with the rise profile is obtained (Fig. 2), and the release of magnetic energy in this run of 5 percent corresponds to 10^{31} erg, a reasonable value for a confined M2-class flare.

The agreement between the observations of the event and our simulation confirms the long-held conjectures that the development of strongly helical axis shapes in the course of eruptions can be regarded as an indication of the kink instabil-

TABLE 1
PARAMETER SETTINGS

Sect.	Simulation Parameters Φ/π	b	$\eta(2)$	L	Scaling Parameters h_0 (Mm)	τ_A (s)	$\lvert\mathbf{B}_0(h_0)\rvert$ (G)	W (erg)
3	5.0	0.29	0.83	10	23	11.5	200	10^{31}
4	–5.0	0.33	1.54	32	115	111	10-40	10^{31-32}

NOTE. — The expression $\eta(z) = -z\,d\ln B_{\rm ex}(0,0,z,0)/dz$ is the 'decay index' of the 'external' field (excluding the contribution by the ring current), L is the box size, and W is the released magnetic energy. The runs are equal in grid resolution in the central part of the box, $\Delta = 0.02$, major rope radius, $R = 1.83$, and distance of the fictitious magnetic charges from the z axis, $l = 0.83$.

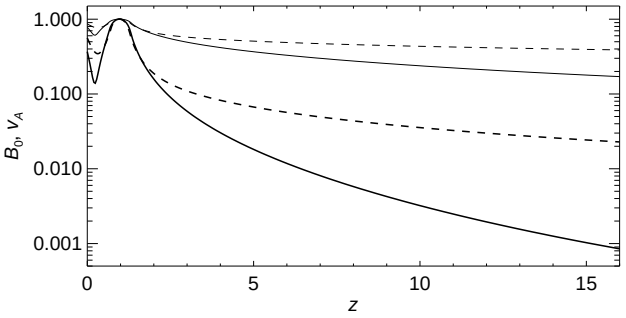

FIG. 3.— Normalized initial magnetic field strength (*thick lines*) and Alfvén velocity (*thin lines*) vs. height for the configurations described in Sect. 3 (original TD model; *dashed lines*) and Sect. 4 (modified TD model; *solid lines*).

ity of a twisted flux rope and that the frequently observed helical fine structures in erupting filaments and prominences outline twisted fields. Furthermore, it shows that flux ropes with substantial twist can exist or be formed in the solar corona at the onset of, or prior to, eruptions.

4. SIMULATION OF AN EJECTIVE ERUPTION (CME)

The full eruption of the kink-unstable flux rope in the TD model is prevented by the strong overlying field, which is dominated by the line current. It is possible to obtain an eruptive behaviour of the flux rope by removing the line current; however, such a modification leads to an infinite number of field line turns at the surface of the flux rope (Roussev et al. 2003). In order to avoid this problem, we replaced the line current by a pair of subphotospheric dipoles (as used in Török & Kliem 2003). The position of the dipoles is chosen such that the field lines of the dipole pair passing through the flux rope match the curvature of the rope as closely as possible. The resulting equilibrium yields a finite twist everywhere in the system, but the magnetic field overlying the flux rope now decreases significantly faster with height than in the original TD model (Fig. 3). By varying the dipole moments or the minor radius b, one can adjust the average twist within the flux rope.

Choosing suitable dipole moments and $b = 0.6$, but otherwise the same parameters of the TD model as in Sect. 3, we first checked that the modified configuration relaxes to a nearby stable equilibrium for subcritical twist, $\Phi = 2.7\pi$. Next a configuration with supercricital twist, $\Phi = -5.0\pi$, is considered, obtained by changing the minor radius to $b = 0.33$ and reversing the dipole moments. The sign of the helicity corresponds to the 2001 May 15 event discussed below; it has no influence on the rise, $h(t)$, of the flux rope apex. The numerical parameters of the simulation are the same as in Sect. 3, except for a considerably larger simulation box and a smaller level of numerical diffusion, which this system permitted.

The helical kink instability also develops in the modified model. However, the flux rope now exhibits a much stronger expansion (Fig. 4), which is not slowed down. The initially exponential rise is followed by a rise with approximately constant and locally super-Alfvénic velocity, until the rope encounters the top of the simulation box (at $t \approx 80$). The helical current sheet remains very weak on top of the flux rope apex and no significant amount of reconnection occurs here. On the other hand, the vertical current sheet now steepens in a large height range. Magnetic reconnection commences in this sheet at the beginning of the exponential phase and rises in tandem with the ascent of the flux rope, particularly closely during the exponential phase. Since the flux rope expands continuously during this phase (instead of being compressed by the upward reconnection outflow below it) and moves away from the forefront of the outflow region afterwards, the ideal instability of the flux rope appears to be the driver of the closely coupled processes. Cusp-shaped field lines are formed throughout the evolution (Fig. 4) but most prominently in the late phase, in agreement with soft X-ray observations of eruptive flares.

The full eruption of the flux rope in the modified TD model must be enabled by the weaker overlying field, since all other parameters are identical, or very close, to Sect. 3.

In Fig. 5 we compare the rise of the flux rope apex in the simulation with the rise of the apex of a well observed eruptive prominence on 2001 May 15, which occurred in a spotless region slightly behind the limb and led to a fast CME (peak velocity of leading edge ≈ 1200 km s^{-1}) and a long-duration flare (X-ray class C4). As described by Maričić et al. (2004), the eruptive prominence developed a helical shape, analogous to the middle panels in Fig. 1 with reversed handedness, and it showed the typical rise characteristics of a fast CME (initially exponential or exponential-like rise, followed by approximately linear rise; Vršnak 2001). For this comparison, we first scaled the Alfvén time such that the duration of the exponential rise phase is matched, $\tau_{\rm A} = 111$ s, and shifted the time axis accordingly. Then we scaled the length unit such that the apex height at the point of peak acceleration in the simulation ($t = 21$) equals the height of the prominence at the resulting observation time (see bottom axis), i.e., $h_0 = 115$ Mm. This fixes the scaling of the velocity and acceleration amplitudes. Apart from a somewhat more gradual decrease of the observed acceleration after the peak, excellent qualitative and quantitative agreement is obtained, demonstrating (as in Sect. 3) that the kink instability yields the growth rate required by the observed rise profile for the twist indicated by the observed helical shape. The slight difference in the late acceleration profile may have many origins, for example, a different height profile of the field strength, or a simultaneous expansion of the overlying field enforced by photospheric flows in the observed event.

The simulation shows a strong magnetic energy release, 25 percent of the initial value, which agrees with the magnitude observed in ejective solar eruptions (Forbes 2000; Emslie et al. 2004). The considered event may have released magnetic energy of order $\sim (10^{31}$–$10^{32})$ erg (the low X-ray class resulted from footpoint occultation). Using the above scaling for h_0, this energy release is reproduced for $B_0 \sim$

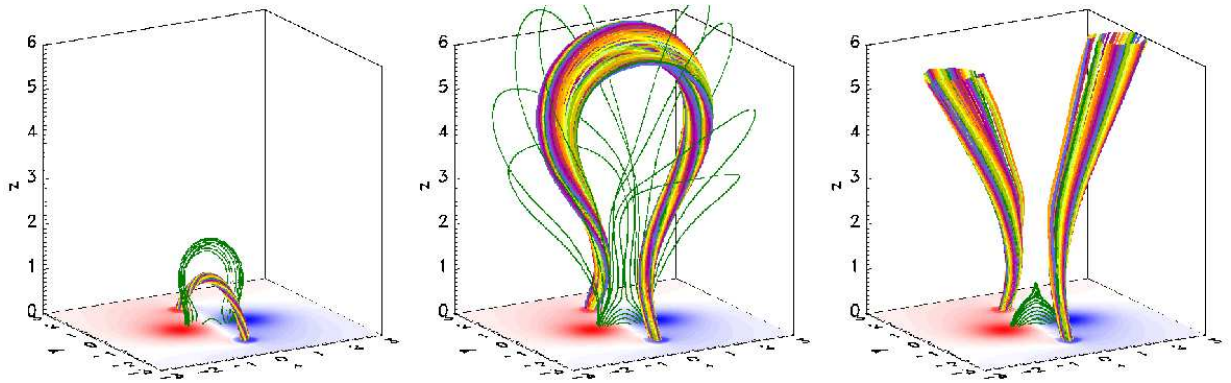

FIG. 4.— Magnetic field lines of the kink-unstable modified TD model at $t = 0$ (*left*), $t = 30$ (*center*), and $t = 43$ (*right*). The magnetogram, $B_z(x,y,0,t)$, is included. Field lines started at a circle of radius $b/3$ in the bottom plane show the core of the flux rope. Additional green field lines, also with identical start points in all panels, indicate the formation of "post flare loops" with a cusp by reconnection. The hyperbolic point of the field at the z-axis (magnetic X-point) lies at $z \approx 0.2$, 0.6, and 1.1, respectively.

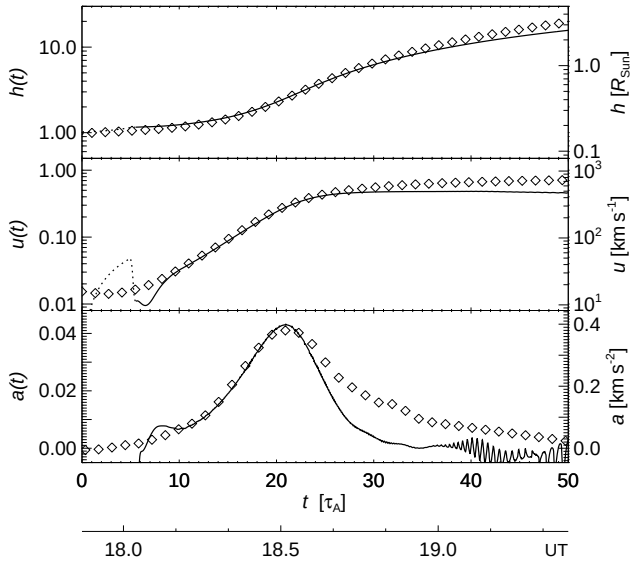

FIG. 5.— Comparison of the simulation in Sect. 4 with the CME on 2001 May 15 in the same format as in Fig. 2, including the acceleration $a(t)$. Diamonds show the apex motion of the erupting prominence/the CME core (data are from Fig. 6a, c of Maričić et al. [2004]).

(10–40) G, consistent with expected averages of the coronal field strength over the large length scales involved.

The simulation could also be scaled to a filament eruption that was associated with an X-class flare and a very fast CME (on 2004 November 10; see Williams et al. 2005).

A line-tied flux rope was found to erupt in a few previous simulations (Amari et al. 2000, 2003a,b). The present simulations, through their agreement with characteristic properties of solar eruptions, *identify a mechanism* for the process, confirming the original suggestion by Sakurai (1976). They also demonstrate the importance of the height dependence of the overlying field for the evolution of the instability into a CME, while Amari et al. (2003b) found the amount of magnetic helicity to be essential. Since Amari et al. built up the helicity by rotating the main photospheric polarities, which simultaneously expands the overlying field (Török & Kliem 2003), both results are fully consistent with each other.

5. CONCLUSIONS

Our MHD simulations of the kink instability of a coronal magnetic flux rope reproduce essential properties—an initially exponential rise with the rapid development of a helical shape—of two well observed solar eruptions, one of them confined, the other ejective. The subsequent approximately linear rise of the ejective eruption is reproduced as well. Since these features are characteristic properties of many solar eruptions (Vršnak 2001), we regard the kink instability of coronal magnetic flux ropes as the initiation mechanism and initial driver of many such events. A sufficiently steep decrease of the magnetic field with height above the flux rope permits the process to evolve into a CME.

We acknowledge constructive comments by the referee and thank H. Ji and B. Vršnak for the observation data in Figs. 2 and 5, respectively. This work was supported by grants 50 OC 9706 (DLR), MA 1376/16-2 (DFG), and HPRN-CT-2000-00153 (EU). The John von Neumann Institute for Computing, Jülich granted computer time.

REFERENCES

Amari, T., et al. 2003a, ApJ, 585, 1073
Amari, T., et al. 2003b, ApJ, 595, 1231
Amari, T., Luciani, J. F., Mikic, Z., & Linker, J. 2000, ApJ, 529, L49
Emslie, A. G., et al. 2004, J. Geophys. Res., 109, A10104
Fan, Y., & Gibson, S. E. 2003, ApJ, 589, L105
Fan, Y., & Gibson, S. E. 2004, ApJ, 609, 1123
Forbes, T. G. 2000, J. Geophys. Res., 105, 23 153
Gerrard, C. L., & Hood, A. W. 2003, Sol. Phys., 214, 151
Hood, A. W., & Priest, E. R. 1981, Geophys. Astrophys. Fluid Dyn., 17, 297
Ji, H., et al. 2003, ApJ, 595, L135
Kliem, B., Titov, V. S., & Török, T. 2004, A&A, 413, L23 (Paper II)
Maričić, D., Vršnak, B., Stanger, A. L., & Veronig, A. 2004, Sol. Phys., 225, 337
Roussev, I. I., et al. 2003, ApJ, 588, L45
Rust, D. M. 2003, Adv. Space Res., 32, 1895
Sakurai, T. 1976, PASJ, 28, 177
Shibata, K. 1999, Ap&SS, 264, 129
Titov, V. S., & Démoulin, P. 1999, A&A, 351, 707 (TD)
Török, T., & Kliem, B. 2003, A&A, 406, 1043
Török, T., Kliem, B., & Titov V. S. 2004, A&A, 413, L27 (Paper I)

Vršnak, B. 2001, J. Geophys. Res., 106, 25 249
Williams, D. R., Török, T., Démoulin, P., van Driel-Gesztelyi, L., & Kliem, B. 2005, ApJ, 628, L163